J Ginseng Res 45 (2021) 228–235

Contents lists available at ScienceDirect

Journal of Ginseng Research

journal homepage: http://www.ginsengres.org

Research Article

Characterization of ginsenoside compound K loaded ionically cross-linked carboxymethyl chitosan–calcium nanoparticles and its cytotoxic potential against prostate cancer cells

Jianmei Zhang [1,☆], Jinyi Zhou [1,☆], Qiaoyun Yuan [1], Changyi Zhan [1], Zhi Shang [1], Qian Gu [1], Ji Zhang [1,***], Guangbo Fu [2,**], Weicheng Hu [1,*]

[1] Jiangsu Collaborative Innovation Center of Regional Modern Agriculture & Environmental protection, Jiangsu Key Laboratory for Eco-Agricultural Biotechnology around Hongze Lake, Huaiyin Normal University, Huaian 223300, China
[2] Department of Urology, The Affiliated Huaian No.1 People's Hospital of Nanjing Medical University, Huaian, 223300, China

ARTICLE INFO

Article history:
Received 2 June 2019
Received in Revised form
24 January 2020
Accepted 30 January 2020
Available online 5 February 2020

Keywords:
Carboxymethyl chitosan
Cytotoxicity
Ginsenoside compound K
Ionic cross-linking
Prostate cancer cell

ABSTRACT

Backgroud: Ginsenoside compound K (GK) is a major metabolite of protopanaxadiol-type ginsenosides and has remarkable anticancer activities *in vitro* and *in vivo*. This work used an ionic cross-linking method to entrap GK within O-carboxymethyl chitosan (OCMC) nanoparticles (Nps) to form GK-loaded OCMC Nps (GK–OCMC Nps), which enhance the aqueous solubility and stability of GK.
Methods: The GK–OCMC Nps were characterized using several physicochemical techniques, including x-ray diffraction, transmission electron microscopy, zeta potential analysis, and particle size analysis via dynamic light scattering. GK was released from GK–OCMC Nps and was conducted using the dialysis bag diffusion method. The effects of GK and GK–OCMC Nps on PC3 cell viability were measured by using the 3-(4,5-dimethyl-2-thiazolyl)-2,5-diphenyl-2-H-tetrazolium bromide assay. Fluorescent technology based on Cy5.5-labeled probes was used to explore the cellular uptake of GK–OCMC Nps.
Results: The GK–OCMC NPs had a suitable particle size and zeta potential; they were spherical with good dispersion. *In vitro* drug release from GK–OCMC NPs was pH dependent. Moreover, the *in vitro* cytotoxicity study and cellular uptake assays indicated that the GK–OCMC Nps significantly enhanced the cytotoxicity and cellular uptake of GK toward the PC3 cells. GK–OCMC Nps also significantly promoted the activities of both caspase-3 and caspase-9.
Conclusion: GK–OCMC Nps are potential nanocarriers for delivering hydrophobic drugs, thereby enhancing water solubility and permeability and improving the antiproliferative effects of GK.

1. Introduction

Ginseng (*Panax ginseng*) has been known as the "king of herbs" since ancient times in eastern Asia. It is a perennial herb that grows in cool habitats and belongs to Araliaceae [1]. As a traditional medicine resource, ginseng extracts have been used to improve immunity and memory and enhance antifatiguing and antiaging capabilities [2,3]. Ginsenosides are the main essential bioactive ingredients in ginseng and can be broadly separated into two categories of protopanaxadiols (Rd, Rc, Rg3, Rb1…) and protopanaxatriols (Re, Rh1, Rg1, Rg2…) [4,5]. Of these, ginsenoside compound K (GK) has received much attention mainly owing to its characteristic pharmacological properties. GK is an intestinal bacterial metabolite of several protopanaxadiols-type ginsenosides (Rb1, Rb2, and Rc) [6]. When high-molecular-weight ginsenosides are degraded in the intestine, GK is absorbed into the systemic

* Corresponding author. Jiangsu Collaborative Innovation Center of Regional Modern Agriculture & Environmental protection, Jiangsu Key Laboratory for Eco-Agricultural Biotechnology around Hongze Lake, Huaiyin Normal University, Huaian, 223300, China.
** Corresponding author. Department of Urology, The Affiliated Huaian No.1 People's Hospital of Nanjing Medical University, 1 Huanghe West Road, Huaian, 223300, China.
*** Corresponding author. Jiangsu Collaborative Innovation Center of Regional Modern Agriculture & Environmental protection, Jiangsu Key Laboratory for Eco-Agricultural Biotechnology around Hongze Lake, Huaiyin Normal University, Huaian, 223300, China.
E-mail addresses: zhangji@hytc.edu.cn (J. Zhang), fgb200@vip.163.com (G. Fu), hu_weicheng@163.com (W. Hu).
☆ These authors equally to this work.

https://doi.org/10.1016/j.jgr.2020.01.007
p1226-8453 e2093-4947/$ – see front matter

circulation in large amounts compared with other ginsenosides, and it has demonstrated such diverse intriguing pharmacological properties such as antiaging, antiangiogenesis, antidementia, antiinflammatory, antidiabetic, and neuroprotective effects [7,8]. It also has a strong cytotoxic effect on PC9 lung cancer, HT29 colon cancer, MCF-7 breast cancer, and HepG2 liver cancer cells by inhibiting cell proliferation, metastasis, and invasion and promoting apoptosis [9–12]. Despite these promising features, the poor water solubility and low permeability of GK greatly reduce its efficacy and thus limit its clinical application [13]. To solve this problem, various nanodelivery systems such as nanoparticles (Nps), micelles, and liposomes have been explored for efficient delivery of hydrophobic drugs [14–17]. Common carriers include polysaccharides, albumin, polyethylene glycol, and lipids, among which chitosan has received extensive attention owing to its nontoxicity and excellent biocompatibility and biodegradability [18]. Carboxymethyl chitosan (CMC) is a biocompatible, biodegradable derivative of chitosan in which free carboxylic groups on the CMC molecular chains are cross-linked with other residuals that can be used to control drug release [19,20]. Moreover, preparing CMC Nps by cross-linking has the advantages of simplicity, greenness, and high efficiency compared with other methods. As a consequence, the application of salts as nontoxic cross-linkers has been investigated in clinical and medical studies [19].

We hypothesized that a nanodrug-loading system would improve the efficiency of drug delivery. Therefore, we prepared O-carboxymethyl chitosan (OCMC) Nps loaded with GK to examine the delivery of GK to PC3 cells and whether antiproliferative activity is enhanced. In this study, OCMC Nps were prepared by the cross-linking method using OCMC as the raw material and calcium chloride ($CaCl_2$) as the cross-linker to encapsulate the GK, thus improving its water solubility and bioavailability and enhancing the antiproliferative activity of GK. PC3 cells were used as a model to evaluate cytotoxicity and cellular uptake in vitro. Further, we expect that the OCMC NPs loaded with GK (GK–OCMC NPs) would have a uniform particle size distribution, which might facilitate cellular uptake and inhibit cancer cell proliferation. To our knowledge, this is the first study to explore the antiproliferative characteristics of GK–OCMC NPs and find potential applications in prostate cancer treatment.

2. Materials and methods

2.1. Materials

GK was provided by Chengdu Must Bio-Technology Co., Ltd (Sichuan, China). Dullbecco's modified eagle's medium (DMEM) and penicillin-streptomytin was acquired from Gibco (Thermo Fisher Scientific, Grand Island, Shanghai, China). Phosphate-buffered saline (PBS) tablets were purchased from Amresco (Solon, OH, USA). 4′6-Diamidino-2-phenylindole was purchased from Sigma (St. Louis, MO, USA). 3-(4,5-Dimethyl-2-thiazolyl)-2,5-diphenyl-2-H-tetrazolium bromide (MTT) was from Biofroxx (Einhausen, Hessen, Germany). Trypsin-ethylenedimainetetraacetic acidwas obtained from Gibco (Burlington, Ontario, Canada). Fetal bovine serum was purchased from Corning (Medford, MA, USA). Cy5.5 NHS ester was purchased from Ruixibio (Xi'an, China). Calcium chloride ($CaCl_2$) was purchased from China Pharmaceutical Group Chemical Reagent Co., Ltd. (Shanghai, China). Caspase-3 and caspase-9 activity assay kits were purchased from Beyotime Biotechnology (Haimen, China).

2.2. Characteristics of O-CMC

Low-molecular-weight OCMC was purchased from Qingdao Honghai Bio-Technology Co., Ltd (Shanghai, China). The OCMC studies are shown in Table 1, along with its molecular weight (Mw) and the degree of carboxymethyl substitution. The Mw of OCMC was determined by Agilent 1260 gel permeation chromatography. A TSK G3000-PWXL column was used for separation with a mobile phase of 0.2 M CH_3COOH and 0.1 M CH_3COONa. The flow rate was set at 0.8 mL/min. The degree of carboxymethyl substitution of the carboxymethyl group of OCMC was determined by potentiometric titration method using a DELTA-320-S pH meter (Shanghai, China).

Table 1
Characterization of O-carboxymethyl chitosan (OCMC)

Sample	Molecular weight (Mw)	Degree of substitution (DS)
O-carboxymethyl chitosan (OCMC)	8600 Da	92%

2.3. Preparation of blank Nps, GK–OCMC Nps, and Cy5.5 labeled GK Nps

GK–OCMC Nps and blank Nps were prepared via an ionic cross-linking method with some modifications [21]. Briefly, 10 mg OCMC was dissolved in 5 mL ultrapure water with stirring for 30 min and then mixed with 1 mL different amounts of GK solution (1:10, 2:10, or 3:10 w/w of OCMC in methanol). Then, 5 mg $CaCl_2$ solution (1 mg/mL) was added dropwise at a speed of 20 drops/min under constant stirring for 30 min at room temperature. Finally, the mixture was dialyzed against distilled water for 24 h through a dialysis bag (Mw cut-off 3.5 kDa) to remove the unencapsulated drug and methanol from the Nps. The solution was freeze-dried to obtain GK–OCMC Nps. Cy5.5 labeled and blank Nps were prepared following the same steps.

2.4. Evaluation of nanoparticle characterization: x-ray diffraction, particle size, zeta potential, and morphology

X-ray diffraction (XRD) patterns of GK, OCMC, and GK–OCMC were acquired by a Rigaku Ultimate IV X-ray diffractometer scanned at speed of 5°/min with ranging from 5° to 80°. The particle size and zeta potential of the GK–OCMC Nps were determined using dynamic light scattering (DLS) with the Nano-ZS90 Malvern Zetasizer (Malvern, UK) in triplicate at 25°C. The morphology of the GK–OCMC Nps was observed under a Tecnai G2 Spirit transmission electron microscope (FEI, USA) after negative staining with 2% (w/v) phosphotungstic acid. Furthermore, the surface characteristics of the Nps were reconfirmed by the NTEGRA Prima atomic force microscope (Nt-Mdt, Zelenograd, Russia), while Nova RC1 software (V1.0.26.1138, Nt-Mdt, Russia) was used for formation of images.

2.5. Drug loading and encapsulation efficiency

The concentration of GK in the Nps was measured via Agilent 1290 Infinity ultrahigh-performance liquid chromatography (UHPLC; Santa Clara, CA, USA). A reversed-phase column (Agilent 1.8 μm SB-C18, 50 mm × 3.0 mm) was used for the separation. The following gradient elution was used: 0–6 min, 57–58% acetonitrile and 6–9 min, 58–70% acetonitrile with a mobile phase of acetonitrile and water. The flow rate was 0.4 mL/min and the ultraviolet wavelength was set to 203 nm. A 1 mg aliquot of the GK–OCMC Nps was dissolved in 1 mL acetonitrile with sonication for 30 min to insure complete dissolution. Subsequently, the solution was detected by UHPLC after filtration through a 0.45 μm membrane filter. Drug loading (DL) and encapsulation efficiency (EE) of the Nps were calculated using formulas (1) and (2):

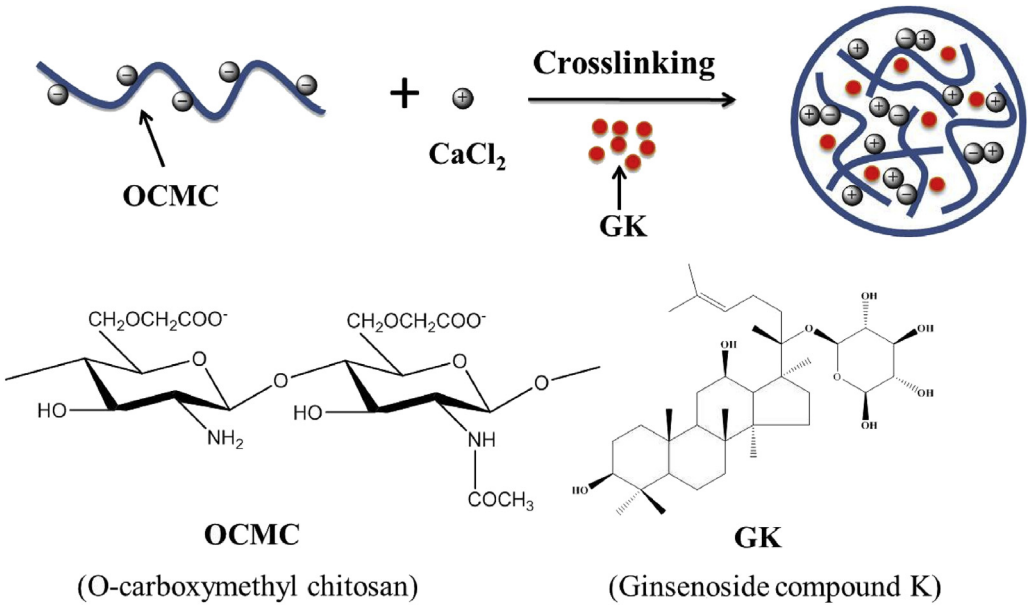

Fig. 1. Schematic representation of the preparation of ginsenoside compound K O-carboxymethyl chitosan (GK–OCMC) nanoparticles (Nps).

$$\text{DL}\ (\%) = \frac{Weight\ \ of\ \ loaded\ \ GK}{Weight\ \ of\ \ namoparticles} \times 100 \quad (1)$$

$$\text{EE}\ (\%) = \frac{Weight\ \ of\ \ loaded\ \ GK}{Weight\ \ of\ \ GK\ \ in\ \ feed} \times 100 \quad (2)$$

2.6. In vitro drug release

The GK was released from the GK–OCMC Nps using the dialysis bag diffusion method. A dialysis bag with a Mw cutoff of 3.5 kDa containing 5 mg GK–OCMC Nps was placed in 40 mL PBS (1% w/v Tween 80) buffer at different pH values (pH 7.4 and 5.8, respectively). The solution was incubated with uninterrupted shaking at 100 rpm in a water bath at 37°C. At particular time intervals (4, 12, 24, 48, 72, and 96 h), 1 mL incubation medium was taken out for subsequent UHPLC measurements and an equal volume of fresh PBS buffer was immediately added for replenishment.

2.7. Cell culture

PC3 cells were obtained from China Center for Type Culture Collection (Beijing, China). PC3 cells were cultured in DMEM containing 10% fetal bovine serum, 100 U/mL penicillin, and 0.1 mg/mL streptomycin in 5% CO_2 at 37°C.

2.8. In vitro cytotoxicity evaluation

The effects of GK and GK–OCMC Nps on PC3 cell viability were measured using the MTT assay previously described [22]. Briefly, the cells were seeded in 96-well plates (2×10^5 cells/well) and cultured for 16–20 h (5% CO_2, 37°C). Next, the cells were treated with GK and GK–OCMC Nps at GK concentrations of 5, 10, 20, 25, and 30 μg/mL in 100 μL fresh DMEM medium for an additional 24 h. Subsequently, 100 μL serum-free medium containing 0.5 mg/mL MTT was added to each well. After 4 h incubation, the purple formazan crystals were dissolved in 100 μL MTT stop buffer solution. Finally, the 96-well plates were placed in a microplate multi-well reader (Infinite M200 Pro, Tecan, Basel, Switzerland) to measure absorbance at 550 nm.

2.9. Cellular uptake assay

PC3 cells (3×10^5 cells/well) were maintained in six-well plates and incubated at 37°C overnight. Then the cells were treated with Cy5.5-labeled GK–OCMC Nps for the indicated times, fixed in 4% formaldehyde for 15 min, and then stained with 2 μg/mL 4′6-diamidino-2-phenylindole in PBS for an additional 15 min. The cells were washed with PBS and observed under a laser confocal microscope (LSM700; Carl Zeiss, Oberkochen, Germany) and analyzed using the Zeiss ZEN 2.3 lite software (Carl Zeiss, Oberkocken, Germany).

2.10. Caspase-3, caspase-9 activity assay

Briefly, PC3 cells (5×10^5 cells/well) were maintained in six-well plates and incubated at 37°C overnight. Then the cells were treated with GK and GK–OCMC Nps at a GK concentration of 30 μg/mL. The activities of caspase-3 and caspase-9 were quantified by a colorimetric assay kit according to the manufacturer's instructions. The absorbance was measured at 405 nm with a multi-well reader (Infinite M200 Pro, Tecan, Basel, Switzerland).

2.11. Data analysis

The values are presented as the mean ± standard deviation. The experimental and control groups were compared using one-way analysis of variance followed by a Student t test and p-values <0.05 were considered significant.

3. Results and discussion

3.1. Characterization of OCMC Nps and GK–OCMC Nps

Several recent studies have described the preparation of chitosan Nps using ionic cross-linking, inverse emulsion, covalent cross-linking, emulsion cross-linking, composite coagulation, solvent evaporation, and polymer dispersion. Of these, ionic cross-linking is

the most widely reported method, and NPs produced using this method exhibit attractive properties [23–25]. The advantages of ionic cross-linking are that it is rapid, safe, reproducible, and easy to scale up. OCMC Nps and GK–OCMC Nps were synthesized via chemical ionic cross-linking between the carboxyl groups of OCMC and the Ca^{2+} ions of $CaCl_2$. The schematic diagram in Fig. 1 shows the main steps in this procedure. The concentrations of the polymer and cross-linker were the major factors affecting the formation of the Nps. Some researchers have reported that OCMC/$CaCl_2$ forms Nps only at weight ratios from 2:1 to 10:1 [26,27]. Preliminary experiments examined the formation of the Nps using various concentrations (0.5, 1, 2, and 3%, w/t) of CMC and (0.5, 1, and 2% w/t) $CaCl_2$ at different mass ratios. The 2:1 ratio was considered the best formulation based on their charge, size, and EE; we also found that the concentrations of OCMC and $CaCl_2$ should be < 2 mg/mL and 1.0 mg/mL, respectively (data not shown). Moreover, the OCMC and $CaCl_2$ concentrations within these ranges had little effect on the polydispersity index of the Nps.

3.1.1. Physical characterization of GK–OCMC Nps

The physical nature of the encapsulated GK Nps was assessed by comparing the XRD patterns of GK, OCMC, and GK–OCMC Nps (Fig. 2). GK displayed a series of significant characteristic crystalline peaks of 2θ at 6.1°, 6.7°, 9.3°, 10.5°, 12.4°, 13.6°, 15.4°, 16.8°, 18.6°, 21.0°, and 22.1°. The OCMC diffraction pattern consisted of a single peak at 21.8°, which was attributed to an amorphous state [28]. After $CaCl_2$ cross-linking, the primary diffraction peak site was retained for GK–OCMC Nps but the peak intensity decreased markedly due to the intermolecular interaction between GK and OCMC in GK–OCMC Nps [26]. This implied that the Nps loaded with GK were successfully prepared.

3.1.2. Nanoparticle size

The particle size of the OCMC Nps and GK–OCMC Nps at different drug/carrier weight ratios was measured using DLS. This showed that the average OCMC NP size was 107.8 ± 4.66 nm (Table 1). After loading GK, the GK–OCMC Nps were also smaller with good dispersibility (Fig. 3A). When the feed weight ratio of GK to OCMC was 3:10, the mean particle size and polydispersability index of the Nps were 173.0 ± 0.71 nm and 0.292 ± 0.029 nm, respectively. The appropriate size was beneficial to escape capture by the reticuloendothelial system leading to higher accumulation of tumor tissues than in normal tissues by the enhanced permeability and retention (EPR) effect [29].

3.1.3. Zeta potential measurements

The charge on the surface of the Nps is critical for the formation of drug-loaded particles because the efficiency of the carrier is proportional to the electrostatic interactions [30]. The surface charge was measured using the zeta potential and the stability of the prepared Nps was evaluated. The zeta potential value of the OCMC Nps was −14.6 ± 0.35 mV (Table 1), indicating that the Nps were negatively charged and stable. The negative charge on the surface of the Nps was attributed to the presence of many COO- groups in OCMC. After the drug was loaded, the zeta potential value of the GK–OCMC Nps was −29.6 ± 0.57 mV (Table 1) and followed a unimodal and concentric distribution (Fig. 3B), indicating that the GK–OCMC Nps exhibited stable dispersibility.

3.1.4. Morphological observation

The surface morphologies of the prepared GK–OCMC NPs were visualized by both transmission electron microscopy (TEM) and atomic force microscopy. As shown in Fig. 3C, they were regular and spherically shaped, with uniform grain diameters and no aggregation. As TEM determined the diameters of the particles in a dry state, the TEM results were slightly smaller than the particle size detected by DLS. The atomic force microscopy images in Fig. 3D and E confirmed the morphologies observed using TEM results. The images clearly show spherical 100–200 nm particles with good dispersion.

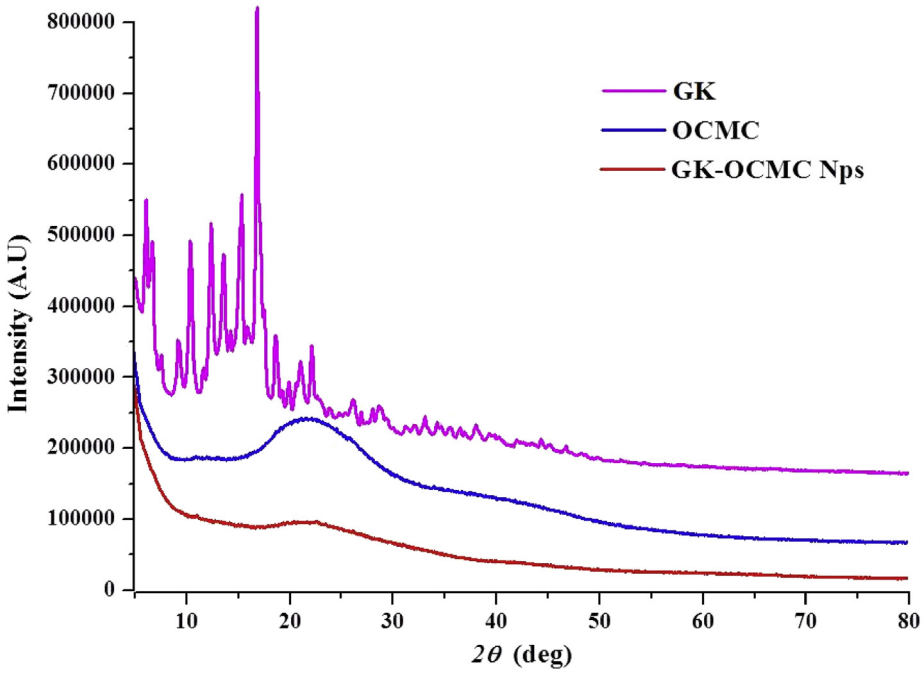

Fig. 2. XRD diffractograms of GK, OCMC, and GK–OCMC Nps.
XRD, x-ray diffraction; GK, ginsenoside compound K; OCMC, O-carboxymethyl chitosan; GK–OCMC, ginsenoside compound K O-carboxymethyl chitosan.

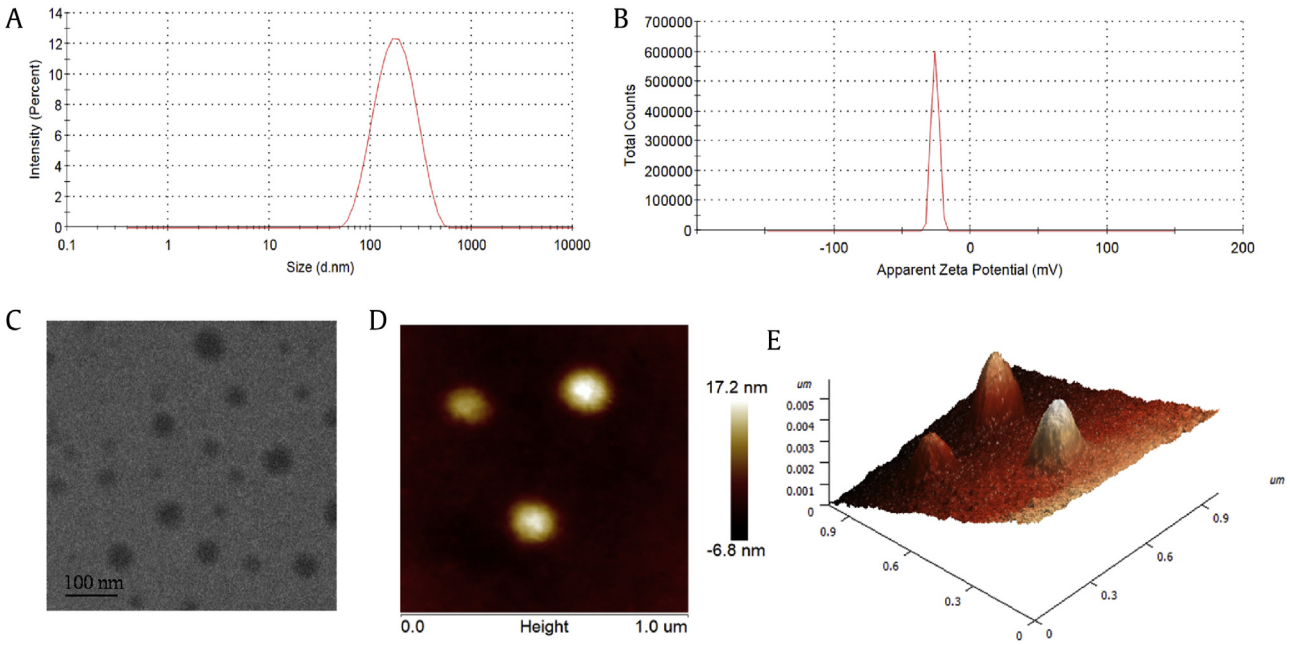

Fig. 3. Characterization of ginsenoside compound K O-carboxymethyl chitosan nanoparticles (GK–OCMC Nps). (A) Size distribution. (B) zeta potential distribution. (C) TEM micrograph. (D) 2 dimensional AFM image. (E) 3 dimensional AFM image.
AFM, atomic force microscopy; TEM, transmission electron microscopy.

Table 2
Characterization of ginsenoside compound K O-carboxymethyl chitosan (GK–OCMC) nanoparticles (Nps)

Sample	Drug/carrier (GK: OCMC)	DL (%)	EE (%)	Diameter(nm)	PDI	Zeta potential(mV)
GK–OCMC	-	-	-	107.8 ± 4.66	0.175 ± 0.048	−14.6 ± 0.35
	1:10	1.95 ± 1.84	5.91 ± 1.24	152.6 ± 2.26	0.246 ± 0.015	−38.4 ± 11.73
	2:10	2.95 ± 0.86	11.10 ± 1.98	261.3 ± 8.34	0.276 ± 0.016	−26.25 ± 0.64
	3:10	4.26 ± 0.73	20.83 ± 2.51	173.0 ± 0.71	0.292 ± 0.029	−29.6 ± 0.57

The data are presented as means ± SD (n = 3).
GK–OCMC, ginsenoside compound K O-carboxymethyl chitosan; DL, drug loading; EE, encapsulation efficiency; SD, standard deviation; PDI, polydispersity index.

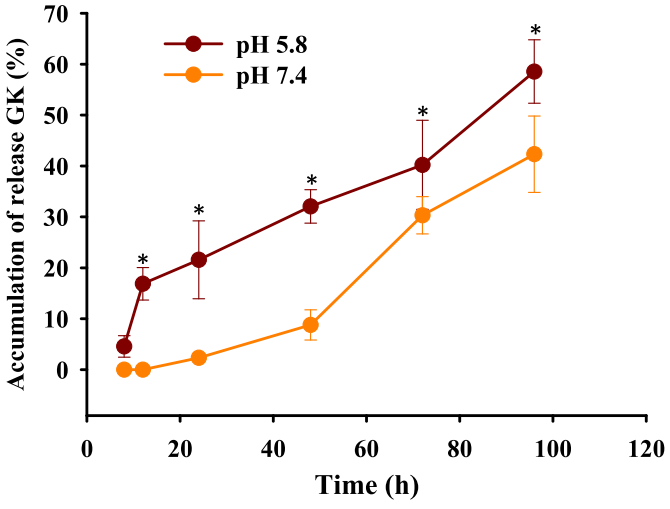

Fig. 4. The controlled release profiles of ginsenoside compound K (GK) from ginsenoside compound K O-carboxymethyl chitosan (GK–OCMC) nanoparticles (Nps) in PBS solution with pH 5.8 and 7.4 at 37°C. The data are presented as means ± SD (n = 3). *$p < 0.05$, significant difference compared with GK within a column.
SD, standard deviation

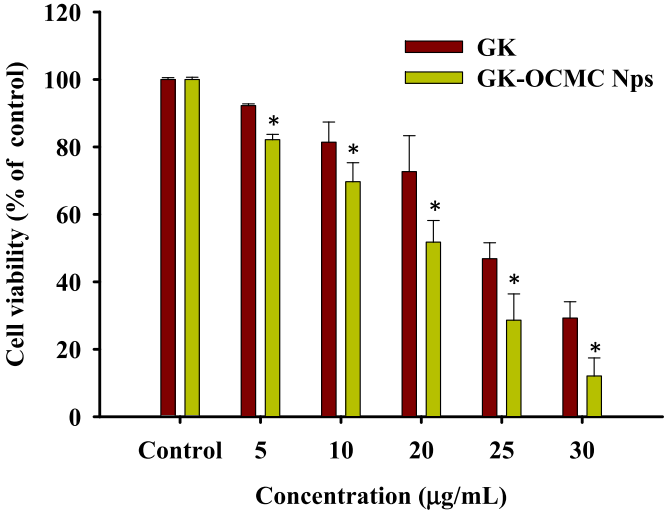

Fig. 5. The cytotoxic effects of ginsenoside compound K O-carboxymethyl chitosan (GK–OCMC) nanoparticles (Nps) and ginsenoside compound K (GK) against PC3 cells. The data are presented as means ± SD (n = 3). *$p < 0.05$, significant difference compared with GK within a column.
SD, standard deviation

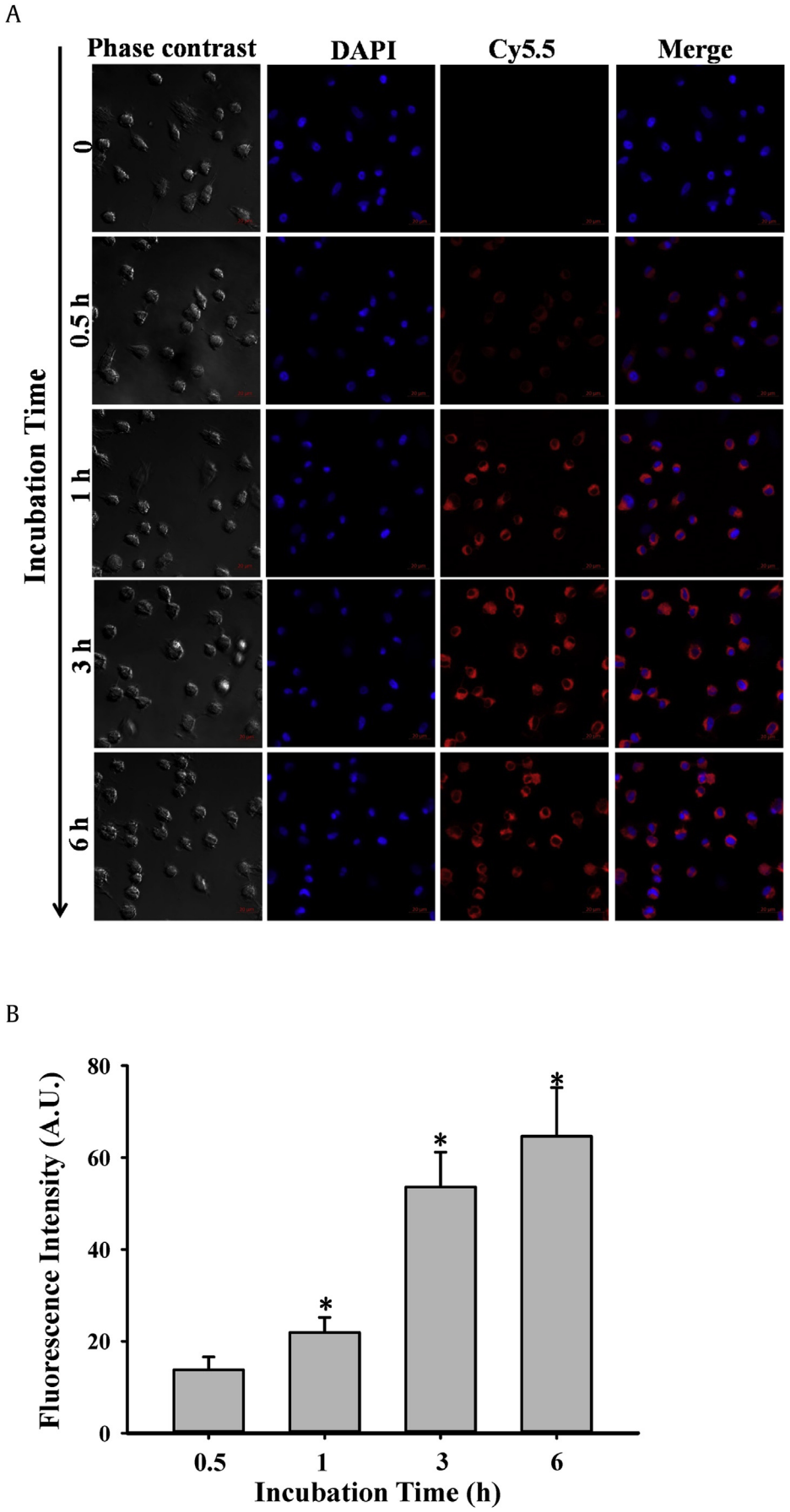

Fig. 6. Confocal fluorescence images of PC3 cells following 0.5, 1, 3, and 6 h of treatment with Cy5.5-labeled ginsenoside compound K O-carboxymethyl chitosan (GK–OCMC) nanoparticles (Nps). *$p < 0.05$, significant difference compared with 0.5 h treatment with Cy5.5-labeled GK–OCMC Nps.

3.2. DL and EE

DL and EE are two important parameters for evaluating drug carriers. As shown in Table 2, as the feed ratio was increased from 1:10 to 2:10, the DL increased from 1.95 ± 1.84% to 2.95 ± 0.86% and the EE increased from 5.91 ± 1.24% to 11.10 ± 1.98%. The DL and EE of GK–OCMC Nps were 4.26 ± 0.73% and 20.83 ± 2.51%, respectively, when the feed ratio of GK and OCMC was further increased to 3:10. These results show that the higher the ratio of drug to carrier and the higher the DL and EE of the Nps, the more potent the drug delivery efficiency of the vectors.

3.3. In vitro release of GK from GK–OCMC Nps

CMC can shield the drug molecules from enzymatic degradation and exhibits physicochemical stability [31]. The release of GK from GK–OCMC Nps may be due to the diffusion of GK and skeleton dissolution behavior [32]. Previous literature showed that the release rate was also related with a drug to polymer ratio, cross-linker concentration, particle size, and charged on the drug and polymer [33]. As shown in Fig. 4, the GK–OCMC Nps exhibited pH-dependent and sustained GK release behavior at pH 5.8 and 7.4. The GK–OCMC Nps released approximately 21.59% of the GK in PBS at pH 5.8 after 24 h, dramatically more than at pH 7.4 (2.34%). Specifically, the release rate of GK was about 58.56% and 42.32% of the total quantity at pH 7.4 and 5.8, respectively, for up to 96 h. Moreover, we found that the drug release rate at lower pH values was consistently higher than that at higher pH values because OCMC swells in an acidic environment due to the protonation of amino groups [33]. These results indicated that the pH-dependent sustained-release pellet would be useful for tumor-targeted drug delivery to extend drug circulation time in the bloodstream.

3.4. In vitro cytotoxicity assay

To explore the potential of GK–OCMC Nps and GK to inhibit cell proliferation, the *in vitro* cytotoxicity of GK–OCMC Nps and GK was estimated in PC3 cells using the MTT assay. As shown in Fig. 5, there was a dose-dependent decrease in PC3 cell viability with the increase in GK–OCMC Nps and the GK concentration required to maintain the same concentration of GK. Specifically, the cell viability after 24 h of incubation with GK–OCMC Nps and GK were 12.11 ± 5.33% and 29.28 ± 4.84 %, respectively, when the concentration of GK–OCMC Nps and GK was 30 μg/mL. The chemical agents encapsulated in drug-loaded nanosystems can effectively migrate into the lysosomes of tumor cells to inhibit tumor cell proliferation and promote cancer cell death [34]. Similarly, chitosan nanocarriers have been used to deliver resveratrol [35], doxorubicin [36], camptothecin [37], and paclitaxel [38]. Consequently, the GK–OCMC Nps appeared to have greater antiproliferative effects than GK, which resulted from the significant cytotoxicity in PC3 cells.

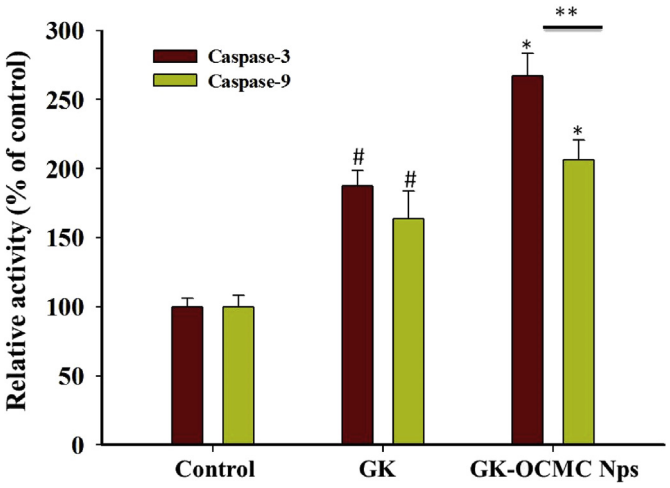

Fig. 7. Effect of ginsenoside compound K O-carboxymethyl chitosan (GK–OCMC) nanoparticles (Nps) and ginsenoside compound K (GK) on the activities of caspase 3 and 9. The data are presented as means ± SD (n = 3). $^{*}p < 0.05$, significant difference compared with GK within a column; $^{\#}p < 0.05$, significant difference compared with control within a column; $^{**}p < 0.05$, significant difference compared with GK and GK–OCMC Nps.
SD, standard deviation

3.5. Cellular uptake

Cellular uptake efficiency of GK–OCMC Nps in PC3 cells was investigated using laser scanning microscopy (LSM) and Cy5.5 as the fluorescent label. As shown in Fig. 6A and B, red fluorescence was rapidly detected for the GK–OCMC Nps in PC3 cells within 30 min and was localized to the cell nucleus after 1 h. Interestingly, the intensity of red fluorescence from the GK–OCMC Nps in PC3 cells strengthened noticeably as incubation time was extended. Thereafter, the nanocarrier was assimilated into cancer cells by a classic endocytosis pathway.

3.6. Caspase-3 and caspase-9 activities

Caspase-9 is an initiator of apoptosis, while caspase-3 is a final executor of tumor growth and progression [39,40]. The caspase-3 and caspase-9 activities were measured using commercial kits. As shown in Fig. 7, GK significantly upregulated the activities of caspase-3 and caspase-9 by 87.56% and 63.45%, respectively, while GK–OCMC treatment enhanced the levels of caspase-3 and caspase-9 by 29.93% and 20.78% compared with that observed with GK treatment.

4. Conclusion

We hypothesized that a nanodrug-loading system would enhance the efficiency of drug delivery. We prepared GK–OCMC NPs by cross-linking CMC and calcium ions. Spherical GK–OCMC NPs with a suitable average particle size and zeta potential were observed. Furthermore, the NPs showed good pH-dependent drug release behavior and higher cytotoxicity and uptake by PC3 cells. These results validate our hypothesis that GK–OCMC NPs enhance uptake and inhibit cell proliferation via the induction of apoptosis; thus, these NPs constitute an efficient system for delivering hydrophobic drugs. Further studies with in vivo models are underway to evaluate the therapeutic efficacy of this system.

Conflicts of interest

The authors declare no conflicts of interest.

Acknowledgments

This study was supported financially by National Natural Science Foundation of China (31600281), Natural Science Foundation of Jiangsu Province (BK20171269), 333 Project of Jiangsu Province (BRA2017241), Natural Science Foundation of the Jiangsu Higher Education Institutions of China (18KJB320001), and Qing Lan Project of Jiangsu Province.

Appendix A. Supplementary data

Supplementary data to this article can be found online at https://doi.org/10.1016/j.jgr.2020.01.007.

References

[1] Hou J, Xue J, Zhao X, Wang Z, Li W, Li X, Zheng Y. Octyl ester of ginsenoside compound K as novel anti-hepatoma compound: synthesis and evaluation on murine H22 cells in vitro and in vivo. Chem Biol Drug Des 2018;91(4):951–6.

[2] Jiménez-Pérez ZE, Singh P, Kim Y-J, Mathiyalagan R, Kim D-H, Lee MH, Yang DC. Applications of *Panax ginseng* leaves-mediated gold nanoparticles in cosmetics relation to antioxidant, moisture retention, and whitening effect on B16BL6 cells. J Ginseng Res 2017;42(3):327–33.

[3] Attele AS, Wu JA, Yuan C-S. Ginseng pharmacology: multiple constituents and multiple actions. Biochem Pharmacol 1999;58(11):1685–93.

[4] Kim SJ, Kim AK. Anti-breast cancer activity of fine black ginseng (*Panax ginseng* Meyer) and ginsenoside Rg5. J Ginseng Res 2015;39(2):125–34.

[5] Patel S, Rauf A. Adaptogenic herb ginseng (*Panax*) as medical food: status quo and future prospects. Biomed Pharmacother 2017;85:120–7.

[6] Hasegawa H, Sung JH, Matsumiya S, Uchiyama M. Main ginseng saponin metabolites formed by intestinal bacteria. Planta Medica 1996;62(5):453–7.

[7] Lee SY. Synergistic effect of maclurin on ginsenoside compound K induced inhibition of the transcriptional expression of matrix metalloproteinase-1 in HaCaT human keratinocyte cells. J Ginseng Res 2018;42(2):229–32.

[8] Kim E, Kim D, Yoo S, Hong YH, Han SY, Jeong S, Jeong D, Kim J-H, Cho JY, Park J. The skin protective effects of compound K, a metabolite of ginsenoside Rb1 from *Panax ginseng*. J Ginseng Res 2018;42(2):218–24.

[9] Yang L, Zhang Z, Hou J, Jin X, Ke Z, Liu D, Du M, Jia X, Lv H. Targeted delivery of ginsenoside compound K using TPGS/PEG-PCL mixed micelles for effective treatment of lung cancer. Int J Nanomedicine 2017;12:7653–67.

[10] Singh P, Singh H, Castro-Aceituno V, Ahn S, Kim YJ, Yang DC. Bovine serum albumin as a nanocarrier for the efficient delivery of ginsenoside compound K: preparation, physicochemical characterizations and in vitro biological studies. RSC Advances 2017;7(25):15397–407.

[11] Li Y, Zhou T, Ma C, Song W, Zhang J, Yu Z. Ginsenoside metabolite compound K enhances the efficacy of cisplatin in lung cancer cells. J Thorac Dis 2015;7(3):400–6.

[12] Wei S, Li W, Yu Y, Yao F, Lixiang A, Lan X, Guan F, Zhang M, Chen L. Ginsenoside Compound K suppresses the hepatic gluconeogenesis via activating adenosine-5'monophosphate kinase: a study *in vitro* and *in vivo*. Life Sci 2015;139:8–15.

[13] Zhang Y, Tong D, Che D, Pei B, Xia X, Yuan G, Jin X. Ascorbyl palmitate/d-alpha-tocopheryl polyethylene glycol 1000 succinate monoester mixed micelles for prolonged circulation and targeted delivery of compound K for antilung cancer therapy *in vitro* and *in vivo*. Int J Nanomedicine 2017;12:605–14.

[14] Muddineti OS, Ghosh B, Biswas S. Current trends in the use of vitamin E-based micellar nanocarriers for anticancer drug delivery. Expert Opin Drug Deliv 2017;14(6):715–26.

[15] de la Puente P, Azab AK. Nanoparticle delivery systems, general approaches, and their implementation in multiple myeloma. Eur J Haematol 2017;98(6):529–41.

[16] Yu H, Teng L, Meng Q, Li Y, Sun X, Lu J, Jl R, Teng L. Development of liposomal Ginsenoside Rg3: formulation optimization and evaluation of its anticancer effects. Int J Pharm 2013;450(1–2):250–8.

[17] Shi Y, Xue J, Jia L, Du Q, Niu J, Zhang D. Surface-modified PLGA nanoparticles with chitosan for oral delivery of tolbutamide. Colloids Surf B Biointerfaces 2018;161:67–72.

[18] Jayakumar R, Menon D, Manzoor K, Nair SV, Tamura H. Biomedical applications of chitin and chitosan based nanomaterials—a short review. Carbohydr Polym 2010;82(2):227–32.

[19] Kalliola S, Repo E, Srivastava V, Heiskanen JP, Sirvio JA, Liimatainen H, Sillanpaa M. The pH sensitive properties of carboxymethyl chitosan nanoparticles cross-linked with calcium ions. Colloids Surf B Biointerfaces 2017;153:229–36.

[20] Berger J, Reist M, Mayer JM, Felt O, Peppas NA, Gurny R. Structure and interactions in covalently and ionically crosslinked chitosan hydrogels for biomedical applications. Eur J Pharm Biopharm 2004;57(1):19–34.

[21] Maya S, Indulekha S, Sukhithasri V, Smitha KT, Nair SV, Jayakumar R, Biswas R. Efficacy of tetracycline encapsulated O-carboxymethyl chitosan nanoparticles against intracellular infections of Staphylococcus aureus. Int J Biol Macromol 2012;51(4):392–9.

[22] Hu W, Wang X, Wu L, Shen T, Ji L, Zhao X, Si CL, Jiang Y, Wang G. Apigenin-7-O-β-D-glucuronide inhibits LPS-induced inflammation through the inactivation of AP-1 and MAPK signaling pathways in RAW 264.7 macrophages and protects mice against endotoxin shock. Food & Function 2016;7(2):1002–13.

[23] Baek J, Wahid-Pedro F, Kim K, Kim K, Tam KC. Phosphorylated-CNC/modified-chitosan nanocomplexes for the stabilization of Pickering emulsions. Carbohydr Polym 2019;206:520–7.

[24] Zhang Y, Thomas Y, Kim E, Payne GF. pH- and voltage-responsive chitosan hydrogel through covalent cross-linking with catechol. J Phys Chem B 2012;116(5):1579–85.

[25] Jain A, Thakur K, Sharma G, Kush P, Jain UK. Fabrication, characterization and cytotoxicity studies of ionically cross-linked docetaxel loaded chitosan nanoparticles. Carbohydr Polym 2016;137:65–74.

[26] Anitha A, Maya S, Deepa N, Chennazhi KP, Nair SV, Tamura H, Jayakumar R. Efficient water soluble O-carboxymethyl chitosan nanocarrier for the delivery of curcumin to cancer cells. Carbohydr Polym 2011;83(2):452–61.

[27] Huang YC, Kuo TH. O-carboxymethyl chitosan/fucoidan nanoparticles increase cellular curcumin uptake. Food Hydrocolloids 2016;53:261–9.

[28] Lu G, Kong L, Sheng B, Wang G, Gong Y, Zhang X. Degradation of covalently cross-linked carboxymethyl chitosan and its potential application for peripheral nerve regeneration. Eur Polym J 2007;43(9):3807–18.

[29] Zhang Z, Wang X, Li B, Hou Y, Yang J, Yi L. Development of a novel morphological paclitaxel-loaded PLGA microspheres for effective cancer therapy: *in vitro* and *in vivo* evaluations. Drug Deliv 2018;25(1):166–77.

[30] Subhapradha N, Shanmugam A. Fabrication of beta-chitosan nanoparticles and its anticancer potential against human hepatoma cells. Int J Biol Macromol 2017;94(Pt A):194–201.

[31] Badran MM, Mady MM, Ghannam MM, Shakeel F. Preparation and characterization of polymeric nanoparticles surface modified with chitosan for target treatment of colorectal cancer. Int J Biol Macromol 2017;95:643–9.

[32] Yadav P, Bandyopadhyay A, Chakraborty A, Sarkar K. Enhancement of anticancer activity and drug delivery of chitosan-curcumin nanoparticle via molecular docking and simulation analysis. Carbohydr Polym 2018;182:188–98.

[33] Khan MA, Zafaryab M, Mehdi SH, Quadri J, Rizvi MM. Characterization and carboplatin loaded chitosan nanoparticles for the chemotherapy against breast cancer *in vitro* studies. Int J Biol Macromol 2017;97:115–22.

[34] Mary Lazer L, Sadhasivam B, Palaniyandi K, Muthuswamy T, Ramachandran I, Balakrishnan A, Pathak S, Narayan S, Ramalingam S. Chitosan-based nanoformulation enhances the anticancer efficacy of hesperetin. Int J Biol Macromol 2018;107(Pt B):1988–98.

[35] Wu J, Wang Y, Yang H, Liu X, Lu Z. Preparation and biological activity studies of resveratrol loaded ionically cross-linked chitosan-TPP nanoparticles. Carbohydr Polym 2017;175:170–7.

[36] Luesakul U, Puthong S, Neamati N, Muangsin N. pH-Responsive Selenium nanoparticles stabilized by folate-chitosan delivering doxorubicin for overcoming drug-resistant Cancer Cells. Carbohydr Polym 2017;181:841–50.

[37] Dramou P, Fizir M, Taleb A, Itatahine A, Dahiru NS, Mehdi YA, Wei L, Zhang J, He H. Folic acid-conjugated chitosan oligosaccharide-magnetic halloysite nanotubes as a delivery system for camptothecin. Carbohydr Polym 2018;197:117–27.

[38] Singh PK, Srivastava AK, Dev A, Kaundal B, Choudhury SR, Karmakar S. 1, 3 β -Glucan anchored, paclitaxel loaded chitosan nanocarrier endows enhanced hemocompatibility with efficient anti-glioblastoma stem cells therapy. Carbohydr Polym 2017;180:365–75.

[39] Lu W, Fu Z, Wang H, Feng J, Wei J, Guo J. Peroxiredoxin 2 is upregulated in colorectal cancer and contributes to colorectal cancer cells' survival by protecting cells from oxidative stress. Mol Cell Biochem 2014;387(1–2):261–70.

[40] Wurstle ML, Laussmann MA, Rehm M. The central role of initiator caspase-9 in apoptosis signal transduction and the regulation of its activation and activity on the apoptosome. Exp Cell Res 2012;318(11):1213–20.